Myosin cleft closure by double electron–electron resonance and dipolar EPR

2007 J. Phys.: Condens. Matter 19 285208

(http://iopscience.iop.org/0953-8984/19/28/285208)

IOP PUBLISHING JOURNAL OF PHYSICS: CONDENSED MATTER

J. Phys.: Condens. Matter **19** (2007) 285208 (10pp) doi:10.1088/0953-8984/19/28/285208

Myosin cleft closure by double electron–electron resonance and dipolar EPR

Piotr G Fajer[1,4], Máté Gyimesi[2], Andras Málnási-Csizmadia[2,3], Clive R Bagshaw[3], K Ilker Sen[1] and Likai Song[1,4]

[1] National High Magnetic Field Laboratory (NHMFL), Institute of Molecular Biophysics, Biology Department, Florida State University, Tallahassee, FL 32306-4380, USA
[2] Eötvös University, Budapest, Hungary
[3] University of Leicester, Leicester, UK

E-mail: fajer@magnet.fsu.edu and song@magnet.fsu.edu

Received 16 October 2006, in final form 7 November 2006
Published 25 June 2007
Online at stacks.iop.org/JPhysCM/19/285208

Abstract

Dipolar electron paramagnetic resonance (EPR) has been used to determine the conformation of the myosin actin-binding cleft in various states of actomyosin ATPase and binding to actin. Comparison of the crystal structures of isolated components and electron microscopy of the actin–myosin complex suggested that the cleft between the upper and lower 50 kDa subdomains closes on binding to actin. The changes in the myosin cleft might be coupled to the state of the nucleotide in the active site and provide communication between ATP hydrolysis and actin binding. In order to detect these changes in solution, we measured the distances between double cysteine mutants of the *Dictyostelium discoidium* myosin II MD by continuous wave EPR and pulsed EPR—double electron–electron resonance (DEER). We have engineered double cysteine mutants C416/C537 which are labelled with spin probes and measured the distances between the upper and lower domains in various nucleotide states and in the presence of actin. We found two major populations of distances at ∼15 Å (conventional EPR) and at 25 Å (DEER) and shifting in the populations as a function of nucleotide state and actin binding, which suggest that the cleft movement is coupled to nucleotides and actin binding and dissociation.

(Some figures in this article are in colour only in the electronic version)

1. Introduction

Myosin is an actin based biological motor responsible for generation of muscle force and various aspects of cell motility. Without myosin animals would not move and cells could not divide or migrate to their target sites. It is reasonable to assume that, as with any motor, the

[4] Address for correspondence: Institute of Molecular Biophysics, Kasha Laboratory, Florida State University, Tallahassee, FL 32306-4380, USA.

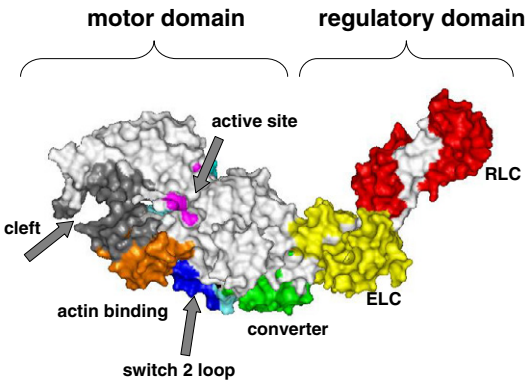

Figure 1. Myosin head structure.

force in myosin is generated by moving parts. Deciphering which parts move, and when, will determine the basic mechanism of this important cellular function. Thanks to x-ray crystallography and electron microscopy, we know the anatomy of the major part of the motor, the myosin head (Rayment *et al* 1993). By comparing myosin head structures in intermediate states of the ATPase cycle we can identify the structural elements that move and might produce force (Geeves and Holmes 1999, Rayment *et al* 1996). However, it is difficult to infer the sequence of events from static crystal structures. Other techniques are needed to study the components in solution, while complexed with other partners and in the presence of the protein dynamics that ultimately drives these transitions. In this paper we set out to (a) corroborate the existence of crystal structure intermediates in solution and (b) determine their structure in actomyosin complexes (the complete motor complex).

1.1. Myosin anatomy

The crystal structure of the myosin head subfragment 1 (S1) reveals two domains: a globular part containing ATP and actin-binding sites—referred to as the *motor domain* (MD)—and an elongated *regulatory domain* (RD) consisting of a long helix with two light chains (the essential light chain (ELC) and the regulatory light chain (RLC)) (see figure 1). On a finer scale, the MD contains:

(a) an active site flanked by three conserved elements found in many ATPases and G-proteins: the *P-loop*, *switch 1* and *switch 2*;
(b) an actin-binding region;
(c) a converter domain forming an insertion socket for the RD;
(d) the *switch 2 helix* the *switch 2 loop* connecting the active site and the converter domain;
(e) a cleft separating the actin-binding site and the upper part of the MD (Geeves and Holmes 1999).

1.2. Geeves and Holmes model for the mechanism of force generation

The structure of S1, with various ATP analogues, shows two distinct conformations: *OPEN* and *CLOSED* (with respect to the active site) (Geeves and Holmes 1999, Rayment *et al* 1996). In the *CLOSED* form there is a tight pocket around γP of ATP and *switch 2* makes a hydrogen bond between γP and G466, (figure 2, right).

A water molecule is positioned for the hydrolysis of ATP and the pocket is stabilized by a salt bridge between *switch 1* and *switch 2*. In the *OPEN* form (figure 2, left), *switch 2* is far from γP, the salt bridge is abolished and the active site is catalytically non-competent

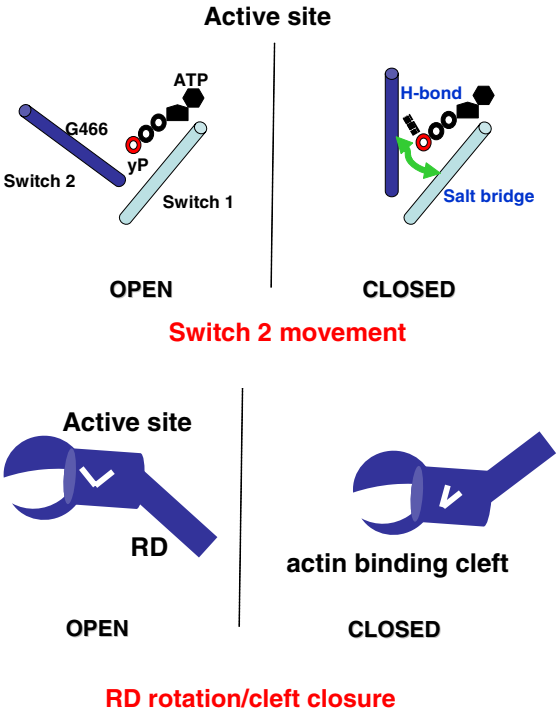

Figure 2. The Geeves and Holmes model of the coupling of the active site and the regulatory domain rotation. Movement of switch 2 closes the active site, ATP is hydrolysed and the regulatory domain swings up.

Figure 3. Changes at the active site.

(Rayment *et al* 1996). Geeves and Holmes (1999) proposed that the transition between the *OPEN* and *CLOSED* conformations, induced by the movement of *switch 2,* is coupled to the large conformational changes depicted in figure 3: (a) rotation of the RD via the *converter* domain and (b) changes to the actin-binding region via closure of the actin-binding cleft.

As the authors stressed, this proposed mechanism accounts for the re-priming of the myosin head when it is detached from actin during a cycle. However, it does not describe the force-generating step because:

(a) force is generated only when myosin is strongly bound to actin while the two structures (*OPEN* and *CLOSED*) have been obtained in the absence of actin;
(b) in both structures, the actin-binding cleft is open preventing strong binding to actin (figure 3).

Most likely *CLOSED* is the initial collision complex with actin while the *OPEN* structure is the '*post-power stroke detached*' state. Force generation needs a third state in between the two (figure 4). This state should have the converter domain and the RD in the down position (post-power stroke), an open γP pocket (post-hydrolysis) and a closed actin-binding cleft that allows strong binding to actin, figure 4.

2. Methods

2.1. Sample preparation

Dictyostelium discoidium (Dd) myosin II motor domain was prepared as described in Conibear *et al* (2003). Briefly, two new cysteines, S416C in the upper 50 K domain and N537C in the lower 50 K domain, were introduced into a cysteine-light construct containing a single buried

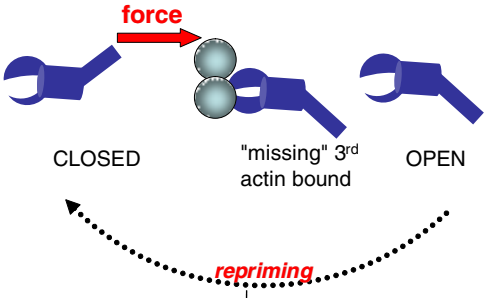

Figure 4. Working hypothesis: (a) do these states exist in solution and (b) does the interconversion between them lead to force generation?

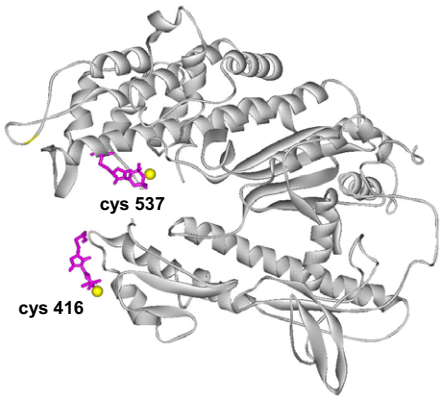

Figure 5. Structure of the Dd MD in the apo state (pdb# 1FMV) with the residues 416 and 537 mutated to cysteines and labelled with MSL. The EPR dipolar interactions arise from the proximity of unpaired electrons denoted as spheres.

cysteine 655 by the megaprimer method in the pDXA-M761 vector. The original cysteine light Dd gene in the pTIKL-Myo vector provided by Spudich laboratory (Shih *et al* 2000), subcloned and its N- and C-termini modified as described in Conibear *et al* (2003). Figure 5 illustrates the position of the cysteine residues 416 and 537 on both sides of the actin-binding cleft. Actomyosin activity was little perturbed in these cysteine mutants as determined in Conibear *et al* (2003).

Prior to labelling the S416C/N537C myosin MD was treated with 10 mM dithiothreitol (DTT) for 30 min at room temperature. DTT was removed by exhaustive dialysis against labelling buffer: 40 mM NaCl, 20 mM 4-(2-hydroxyethyl)-1-piperazineethanesulfonic acid (HEPES), 2 mM $MgCl_2$, pH 7.5. The 40–80 μM protein was then labelled with a 1.5-fold excess of maleimide spin label (MSL; *N*-(1-oxyl-2,2,6,6-tetramethyl-4-peperidinyl)maleimide, Aldrich) in dimethyl formamide (DMF) for 8 h at 0 °C. Unreacted spin label was removed by dialysis. The 80–90% efficiency of labelling was measured by double integration of the EPR signal and bicinchoninic acid (BCA) protein assay. Samples with a labelling efficiency of less than 30% were used as uncoupled controls. Actin was prepared according to Spudich and Watt (1971) and added at four-fold excess to S1. For the experiments below freezing temperatures, 30% sucrose was added to create a frozen glass solution and avoid high local concentrations of protein aggregates created during freezing.

2.2. Electron paramagnetic resonance (EPR) spectroscopy

Two different dipolar EPR methods were used to determine the inter-spin distance:

(a) conventional, continuous wave (cw) EPR, which is sensitive to distances of 8–25 Å (Altenbach *et al* 2001);

(b) the pulsed ERP technique—double electron–electron resonance (DEER)—sensitive to distances in the range of 17–70 Å (Pannier *et al* 2000, Sale *et al* 2005).

EPR spectra were recorded on a Bruker E680 X/W-band pulsed EPR instrument (Bruker Spectrospin, Billerica, MA) operating at 9 GHz. Conventional EPR experiments were performed at 150 K with a modulation frequency of 100 kHz, modulation amplitude 1 G and microwave power of 20 μW. Spectral broadening of the double-labelled samples, compared with the under-labelled samples, was analysed using a Gaussian fitting method developed in our laboratory. DEER experiments were performed at 65 K using a four-pulse sequence with a 16 ns $\pi/2$ pulse. A 65 MHz frequency offset was used for the ELDOR pulse. The DEER spectra were analysed with a Monte Carlo/simplex Gaussian convolution method. The details and description of the DEER experiments were as given in Fajer *et al* (2006b) with the addition of automatic scanning of the number of Gaussian populations of distances from 1–4. The lowest number of Gaussians is chosen on the basis of the f-test comparing the improvement of χ^2 and the increased number of degrees of freedom. In all cases in this work, both the cw and DEER spectra are best described by a single Gaussian population. The inclusion of a second Gaussian did not improve the fits.

Power saturation was performed at 4 °C in the presence of 5 mM ethylenediamine-N, N'-diacetic acid (NiEDDA) as a relaxant and in the samples saturated with N_2. $P_{1/2}$ was determined by fitting the spectral height variation (A) as a function of increasing incident power (P) to

$$A = \frac{A_o\sqrt{P}}{[1 + (\sqrt[1.5]{2} - 1)\frac{P}{P_{1/2}}]^{1.5}}.$$

2.3. Computational modelling of spin label conformers

The label conformation was estimated using combined Metropolis Monte Carlo rotamer searches and a molecular dynamics approach developed in our laboratory (Fajer *et al* 2006a, Sale *et al* 2002, 2005). The method consists of a two-stage approach in which the structure is first minimized using Charmm19 forcefields, the selected residue is 'mutated' using InsightII Biopolymer module (Accelrys) to a MSL and the conformers of the spin labels are selected by repeated random perturbation of any of the five bonds between the α carbon and the nitroxide ring followed by energy minimization. Each structure generated in this way is subject to the Metropolis criterion and either retained or rejected. The top 300 lowest energy conformers from each labelled site are used to generate 300^2 distances which are then ordered according to their combined energies and Boltzmann weighting. To relieve the constraint of a 'rigid cage' protein environment experienced by the label and map out the local energy landscape around the energy minimum we performed molecular dynamics simulations. The lowest energy conformers were used as a seed to molecular dynamics simulation, heated up to 300 K in 10° steps (2 fs steps), equilibrated for 300 ps using 1 fs steps and subject to a production run of 1 ns (2 fs steps). All the residues within a 15 Å sphere of the spin labels at each site were allowed to move. All the scripts were written and executed in Charmm 27 and are available at http://fajerpc.magnet.fsu.edu and in Fajer *et al* (2006a).

3. Results and discussion

3.1. Solvent accessibility

Qualitatively, the closure of the cleft should be reflected in the solvent exposure of the labelled sites. We used a single cysteine mutant S416C labelled with MSL to measure the exposure to

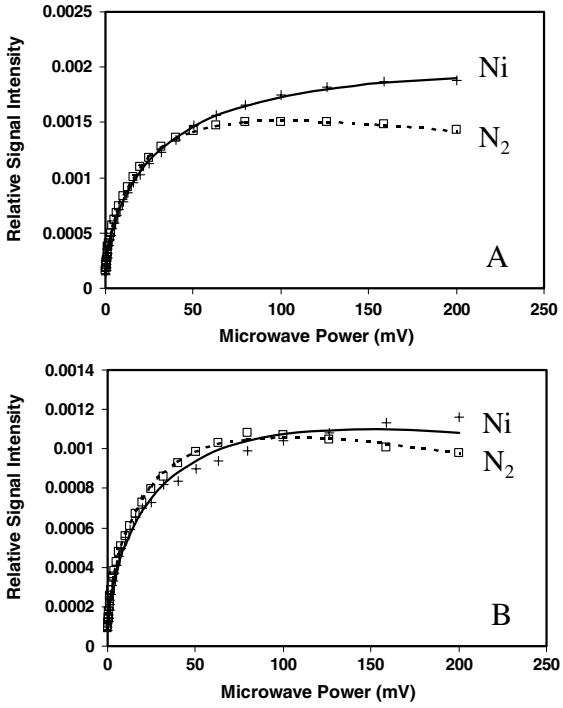

Figure 6. Power saturation curves of the MSL labelled myosin MD. (A) S1 and (B) ActoS1: +, in the presence of a paramagnetic relaxation agent −, 5 mM NiEDDA; □, saturated with nitrogen; solid and dotted lines are non-linear fits. All experiments were performed at 4 °C.

the water soluble relaxation agent NiEDDA. The saturation of nitroxide spin with increasing microwave power, figure 6, can be relieved by cross relaxation to another paramagnetic species if they collide with each other. The change of saturation properties is thus a measure of the probability of collisions and hence exposure to the aqueous environment. The difference between the N_2 saturated samples (N_2 displaces the O_2 which is paramagnetic) and the samples in the presence of NiEDDA is proportional to the exposure of the label to water. As shown in figure 6 and parameterized in table 1 this difference is large in the apo-S1 state and becomes significantly smaller in the presence of actin. For samples with no actin, $P_{1/2}$ half-saturation power, a measure of the relaxation rate, increases by ∼100 mW in the presence of the relaxation-enhancing NiEDDA, but the effect is much smaller (20 mW) when actin is present. This basic result is interpreted as evidence of decreased water accessibility in the presence of actin and shielding of the spin label from the aqueous environment.

3.2. Continuous wave EPR

A more direct measure of cleft conformation is spin–spin distance between the labels on opposite sites of the cleft. The conventional EPR spectra in figure 7 display a considerable broadening over the spectrum of the single cysteine mutant for all nucleotide states. The spectra are fitted with a dipolar function corresponding to a Gaussian distribution of distances centred at 17 Å with a full-width of 6 Å. The small variation of the average distances (16–18 Å) and distribution (7–12 Å), table 2, is comparable to the errors at the 50% confidence level and we do not consider these differences to be significant (for data of this quality). The strongest variation is the fraction of coupled spins (i.e. spins that 'see' each other and generate dipolar broadening); this population increases by 1/3 on actin binding and is consistent with the closure of the cleft. No large changes were observed between the apo and ADP states both of which represent a

Table 1. Aqueous accessibility as measured by power saturation.

Sample	$P_{1/2}$ (mW)
S1 in N_2	109 ± 2
S1 + NiEDDA	206 ± 28
ActoS1 in N_2	109 ± 8
ActoS1 + NiEDDA	127 ± 9

Table 2. Distances determined by DEER and conventional EPR.

	CW EPR			DEER		
Active site state	% coupled	r (Å)	Δr (Å)	% coupled	r (Å)	Δr (Å)
ActoS1	65	18 ± 2	9 ± 3	21	23 ± 3[a]	23 ± 10
Apo	46	16 ± 2	12 ± 3	32	25 ± 2	18 ± 4
ADP	52	16 ± 2	7 ± 3	34	25 ± 2	17 ± 4
AlF_4^-	69	17 ± 2	10 ± 3	29	25 ± 2	17 ± 3

[a] Errors were determined from the contours at $1.7\chi^2$.

post-power stroke, OPEN conformation of the active site. There was, however, a change in the fraction of coupled spins for AlF_4^- state, which mimics the pre power-stroke, CLOSED conformation of the head. The short distance population increased as on actin binding.

3.3. Double electron–electron resonance

Longer distances between the spins, resulting in weaker dipolar broadening can be measured using pulse methods such as DEER in which the dipolar interactions are seen as a modulation of the echo and thus not obscured by the EPR signal itself. The DEER signal modulation is shown in figure 8; the modulation decays monotonically to baseline within 0.2 μs implying that (a) the distances are short (fast decay) and (b) the distribution is wide (the oscillations characteristic of well defined distance distribution are absent).

The analysis of DEER revealed distances of 22–25 Å with a Gaussian width of 17 Å for all states of the nucleotides (table 2). The presence of actin did not appreciably change distance, however the fraction of the spins coupled at longer distance decreased significantly (by a third).

3.4. Molecular modelling

The distances measured by conventional EPR and DEER were compared with the inter-spin distances predicted from the crystal structures in different nucleotide states (pdb# 1FMV, 1MMA, 1MND and a flex-docked structure of the actoS1 complex, (Holmes *et al* 2003), courtesy of Dr R Schroeder). The black bars in figures 7 and 8 represent populations of the distances between the labels for conformers with low energy determined by the Monte Carlo method. The agreement is decent except for the width of the distributions which is narrower in the simulations than is experimentally observed. Since the Monte Carlo simulations select the very lowest energy minima in a rigid protein environment we have performed molecular dynamics simulations to scope the energy surface within the minima available at room temperature as well as relaxation of the 'rigid cage' conditions that might be biasing the rotamer population. These relatively short (1 ns) molecular dynamics simulations are not designed to explore the global rotamer space but rather refine the available space around a MMCM (Metropolis Monte Carlo minimization). Even with this limitation it is obvious that the available rotamer space is larger than predicted from the MMCM alone (shaded bars in

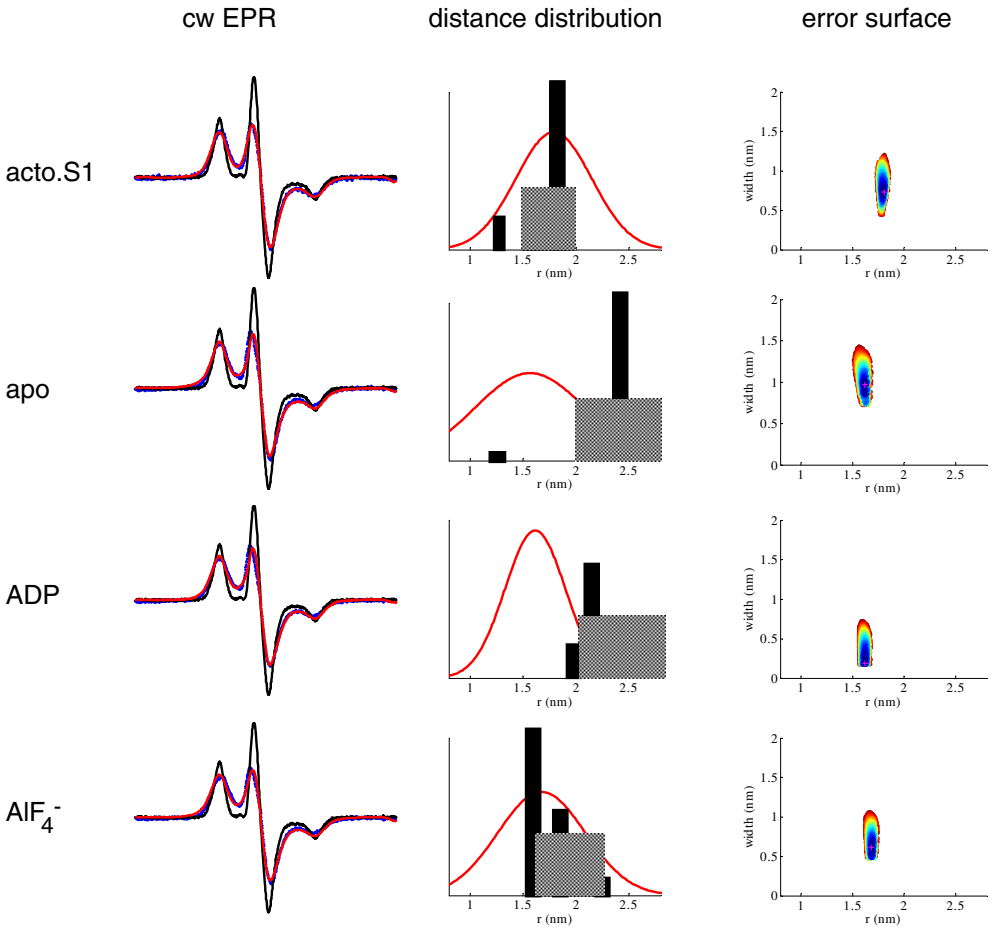

Figure 7. Conventional EPR of cleft mutants. Left: spectra of the under-labelled sample (sharper spectra), double mutant (broader spectra) and the best fit spectra convolving the under-labelled spectrum with the dipolar function corresponding to the Gaussian distribution (middle column). The contour plots in the right column are at $1.7\chi^2$ of the best fit and represent possible solutions in average distance and in width of Gaussian distribution at a confidence limit of 50%. Black and shaded bars in the middle column are distances spanned by Monte Carlo search and molecular dynamics, respectively. Crystal structures 1FMV, 1MMA and 1MND modified with MSL label were used for apo, ADP and AlF_4^- states; the flexible docking structure of actoS1 courtesy of Dr R Schroeder was used for a structure in the presence of actin.

figures 7 and 8). For AlF_4^- and the actoS1 state the agreement between the shorter distance predicted from cw EPR and simulations is better than for the apo and ADP states. Simulations for the latter two states would lead one to expect longer distances (23–25 Å) than those observed by cw EPR (16–18 Å). However, the DEER observed distances coincide with those predicted by simulations.

4. Conclusions

Surprisingly, we did not detect a change in the average distance between the spin labels in the upper and lower 50 K domains of the myosin head on actin binding. We have observed small

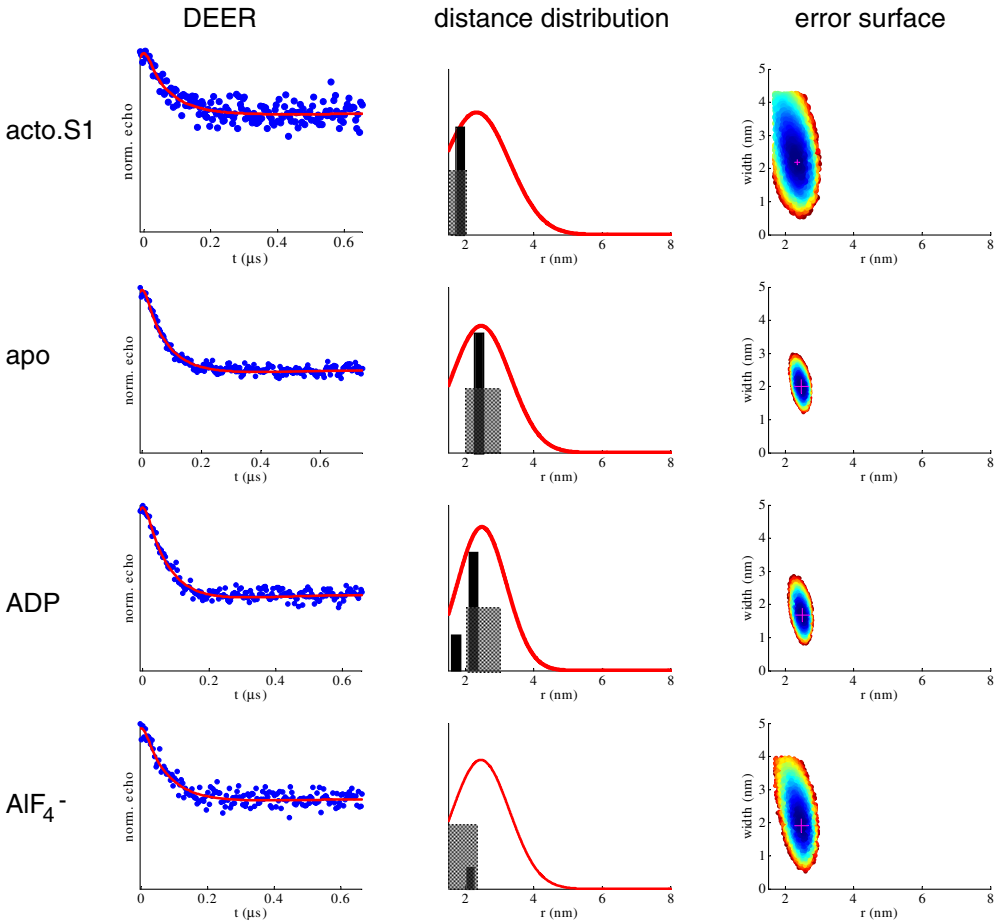

Figure 8. DEER of cleft mutants. Left: DEER dipolar evolution function and the best fit dipolar evolution function corresponding to the Gaussian distribution (the middle column). The contour plots in the right column are at $1.7\chi^2$ of the best fit and represent possible solutions in average distance and in width of Gaussian distribution at a confidence limit of 50%. Black and shaded bars in the middle column are distances spanned by Monte Carlo search and molecular dynamics, respectively, as described in figure 7.

but significant shifts in population of the shorter distances at the expense of longer distances induced by actin.

We can think of two scenarios to explain the combined data in molecular terms. In the first scenario, there are two conformations of the cleft present in equilibrium—binding of actin does not result in a change of distance but rather in change of the relative populations. The smaller modulation depth of the actoS1 complex (figure 8) suggests that the population of longer distances decreases when actin binds. The reverse is also true for shorter distances; the population of spins at short distances increases with actin binding. Thus, *the conformation of the cleft is dynamic in either state, binding of actin changes the equilibrium towards the short distance population consistent with closure of the cleft.*

We cannot rule out an alternative scenario: in this there are two families of the label rotamers, one in which the inter-spin distance is short at 16–18 Å and another one in which labels are at 22–25 Å. Both populations are clearly visible in the simulations of AlF_4^- and apo

states (figure 7). Such populations arise from an upward rotation of the C416 spin label and by rotation of the C537 label towards the entrance of the cleft (figure 5). These rotations are within a few kcal of each other and might be in equilibrium at room temperature. Binding of actin and closure of the cleft will bias the equilibrium towards the shorter distance conformers.

These competing scenarios can be distinguished by variety of approaches currently under way in our laboratory: (a) different mutant pairs that will allow for triangulation of the backbone changes; (b) longer trajectories using more seed points to better sample the label conformer space; (c) utilization of a newly developed '*simulation scaling*' method that varies the magnitude of terms in the Hamiltonian to facilitate replica exchange (Li *et al* 2006). Irrespective of the details of the cleft rearrangement it is clear that actin binding did induce measurable changes in the conformation of the cleft.

Acknowledgments

Dr Elizabeth Fajer is thanked for careful editing of the manuscript. Members of Fajer's laboratory are thanked for many hours of helping to debug the software. This work was sponsored by grants from National Science Foundation MCB 0346650 and the American Heart Association GIA 0455236B to PF, the pulsed EPR instrument was funded by NSF CHE-0079649 to PF. LS and KIS were recipients of the American Heart Association predoctoral fellowships. CRB and AMC acknowledge the support of Wellcome Trust IRDA award (071525) and EMBO/HHMI, Bekessy fellowship, National Office for Research and Technology RET 14/2005, NKFP-012/2005 and Scientific Research Fund OTKA TS049812.

References

Altenbach C, Oh K J, Trabanino R J, Hideg K and Hubbell W L 2001 Estimation of inter-residue distances in spin labelled proteins at physiological temperatures: experimental strategies and practical limitations *Biochemistry* **40** 15471–82

Conibear P B, Bagshaw C R, Fajer P G, Kovacs M and Malnasi-Csizmadia A 2003 Myosin cleft movement and its coupling to actomyosin dissociation *Nat. Struct. Biol.* **10** 831–5

Fajer M, Fajer P G and Sale K L 2006a *Molecular Modeling of Spin Labels* ed M Hemminga and L Berliner (Berlin: Springer)

Fajer P G, Brown L and Song L 2006b *Practical Pulsed Dipolar EPR (DEER)* ed M Hemminga and L Berliner (Berlin: Springer)

Geeves M A and Holmes K C 1999 Structural mechanism of muscle contraction *Annu. Rev. Biochem.* **68** 687–728

Holmes K C, Angert I, Kull F J, Jahn W and Schroder R R 2003 Electron cryo-microscopy shows how strong binding of myosin to actin releases nucleotide *Nature* **425** 423–7

Li H, Fajer M and Yang W 2006 Simulated scaling method for localized enhanced sampling and simultaneous 'Alchemical' free energy simulations: a general method for MM, QM, and QM/MM simulations *J. Chem. Phys.* at press

Pannier M, Veit S, Godt A, Jeschke G and Spiess H W 2000 Dead-time free measurement of dipole–dipole interactions between electron spins *J. Magn. Reson.* **142** 331–40

Rayment I, Holden H M, Whittaker M, Yohn C B, Lorenz M, Holmes K C and Milligan R A 1993 Structure of the actin–myosin complex and its implications for muscle contraction *Science* **261** 58–65

Rayment I, Smith C and Yount R G 1996 The active site of myosin *Annu. Rev. Physiol.* **58** 671–702

Sale K, Sar C, Sharp K A, Hideg K and Fajer P G 2002 Structural determination of spin label immobilization and orientation: a Monte Carlo minimization approach *J. Magn. Reson.* **156** 104–12

Sale K, Song L, Liu Y S, Perozo E and Fajer P 2005 Explicit treatment of spin labels in modelling of distance constraints from dipolar EPR and DEER *J. Am. Chem. Soc.* **127** 9334–5

Shih W M, Gryczynski Z, Lakowicz J R and Spudich J A 2000 A FRET-based sensor reveals large ATP hydrolysis-induced conformational changes and three distinct states of the molecular motor myosin *Cell* **102** 683–94

Spudich J A and Watt S 1971 The regulation of rabbit skeletal muscle contraction. I. Biochemical studies of the interaction of the tropomyosin–troponin complex with actin and the proteolytic fragments of myosin *J. Biol. Chem.* **246** 4866–71